BIOCHEMISTRY
including biophysical chemistry & molecular biology

Article

pubs.acs.org/biochemistry

Helices 2 and 3 Are the Initiation Sites in the $PrP^C \rightarrow PrP^{SC}$ Transition

Jie Chen[†] and D. Thirumalai*[,†,‡]

[†]Biophysics Program, Institute for Physical Science and Technology, and [‡]Department of Chemistry and Biochemistry, University of Maryland, College Park, Maryland 20742, United States

ABSTRACT: It is established that prion protein is the sole causative agent in a number of diseases in humans and animals. However, the nature of conformational changes that the normal cellular form, PrP^C, undergoes in its conversion to a self-replicating state is still not fully understood. The ordered C-terminus of PrP^C proteins has three helices (H1−H3). Here, we use statistical coupling analysis (SCA) to infer covariations at various locations using a family of evolutionarily related sequences and the response of mouse and human PrP^Cs to mechanical force to decipher the initiation sites for the transition from PrP^C to an aggregation-prone PrP* state. Sequence-based SCA predicts that the clustered residues in nonmammals are localized in the stable core (near H1) of PrP^C, whereas in mammalian PrP^C, they are localized in frustrated helices H2 and H3 where most of the pathogenic mutations are found. Force−extension curves and free energy profiles as a function of extension of mouse and human PrP^C in the absence of a disulfide (SS) bond between residues Cys179 and Cys214, generated by applying mechanical force to the ends of the molecule, show a sequence of unfolding events starting first with rupture of H2 and H3. This is followed by disruption of structure in two strands. Helix H1, stabilized by three salt bridges, resists substantial force before unfolding. Force extension profiles and the dynamics of rupture of tertiary contacts also show that even in the presence of an SS bond the instabilities in most of H3 and parts of H2 still determine the propensity to form the PrP* state. In mouse PrP^C with an SS bond, there are ∼10 residues that retain their order even at high forces. Both SCA and single-molecule force simulations show that in the conversion from PrP^C to PrP^{SC} major conformational changes occur (at least initially) in H2 and H3, which because of their sequence compositions are frustrated in the helical state. Implications of our findings for the structural model for the scrapie form of PrP^C are discussed.

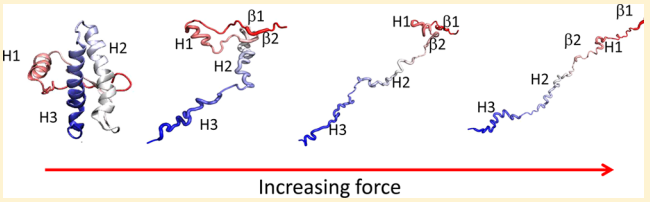

Aggregation of misfolded proteins is implicated in a number of diseases.[1,2] For example, misfolding of the extracellular globular prion proteins, attached to the plasma membrane by a glycosylphosphatidylinositol anchor, is associated with a variety of transmissible spongiform encephalopathies, including bovine spongiform encephalopathy, scrapie disease in sheep, and Creutzfeldt-Jakob disease in humans. Prion disorders [also termed transmissible spongiform encephalopathies (TSEs)] are fatal neurodegenerative diseases that are linked to the misfolding and subsequent aggregation of the normal globular protein PrP^C. According to the "protein only hypothesis",[1,3] the aggregated scrapie form, PrP^{SC}, is the causative agent of the various TSE-linked diseases. The scrapie conformation can recruit the cellular form, PrP^C, and facilitate its conversion to PrP^{SC}, thus ensuring self-propagation.[4] Given the crucial role played by the misfolded states of PrP^C in TSE, it is natural that there has been intense effort in deciphering the mechanism of conversion from the normal cellular form to the PrP^{SC} state.

It is believed that residues 90−231 of PrP^C are the minimal infectious unit. Structures of mammalian as well as non-mammalian PrP^C from a number of species show that residues 90−121 are mostly disordered while the rest of the residues are ordered.[5−7] The structured C-terminal part of PrP^C consists of three helices [H1−H3 (Figure 1)] and two small β-sheets.[5,8] In mouse PrP^C, shown in Figure 1, H1−H3 span residues 144−153, 172−194, and 200−224, respectively. There is no clear structural model for the scrapie form,[9] although most recent studies[10,11] favor a parallel in-register arrangement of a conformationally altered form of PrP^C. It is known that PrP^{SC} has substantial β-strand content, which implies that in the $PrP^C \rightarrow PrP^{SC}$ transition a large-scale conformation rearrangement must occur.

Via integration of several experimental and computational studies, it has been proposed that prion aggregation is preceded by the conversion of PrP^C to a monomeric aggregation-prone state, PrP^{C}*, which unlike in the aggregation of other disease-related proteins such as Aβ,[12] is more stable than PrP^C. In other words, under normal operating conditions, the functional form PrP^C could be metastable.[13] A large free energy barrier (exceeding 20−25 kcal/mol) separates isoforms PrP^C and PrP^{C}*, and hence, the latter is rarely populated during the typical life cycle of PrP^C.[14] A key question involves the regions in PrP^C that harbor residues that are most susceptible to conformational changes in the $PrP^C \rightarrow PrP^{C}$* transition. Several years ago, Dima and Thirumalai (DT)[15,16] proposed that in mammalian prions the core of the ordered C-terminal region of PrP^C is frustrated and the associated instability could trigger an $\alpha \rightarrow \beta$ transition. Frustration implies that the

Received: April 28, 2012
Revised: December 14, 2012
Published: December 20, 2012

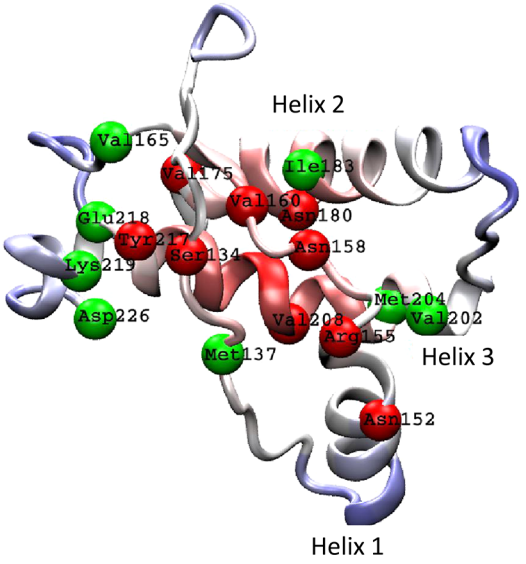

Figure 1. Ribbon diagram of mouse prion (Protein Data Bank entry 1AG2). We show only the structured C-terminal region. The spheres represent the network of covarying residues calculated using the sequence-based statistical coupling analysis. Green and red correspond to mammals and nonmammals, respectively.

secondary structures adopted by certain residues in the native state are incompatible with their natural propensities as assessed by comparison to a database of structures. Using bioinformatics methods, structural analysis, and molecular dynamics simulations, DT showed that conformational fluctuations in the C-terminal end of H2 and in a large portion of H3 are involved in the $PrP^C \rightarrow PrP^{C*}$ transition in mammalian prions.[15,16] Because global conformational change is required to populate the aggregation-prone PrP^{C*} state, the barrier to its formation is large, which explains the rarity of prion disorders during normal function.

Although prion genes are shared by vertebrates, nonmammalian species are apparently not susceptible to prion disorders. By studying the turtle prion protein, Simonic et al. suggested that an α-helix $\rightarrow$ β-sheet transition is unlikely in nonmammals.[17] Using several structural measures and a quantitative assessment of frustration based on the concept that certain sequences are discordant[18] [they adopt a certain secondary structure (α-helix for example) in a protein but would normally have a different structure (β-strand) in a majority of proteins], DT showed that the avian helices are not as frustrated as their mammalian counterparts.[15] This study and a related work[16] rationalized the finding that nonmammalian species typically do not acquire prion disorders.

To provide further insights into the extent of local frustration, we used a sequence-based method to tease out the plausible reasons for the differences in mammalian and nonmammalian PrP^C. In particular, we applied the statistical coupling analysis (SCA) technique[19−21] to extract a network of residues that are evolutionarily important from multiple-sequence alignment of the protein family. We performed SCA for prion proteins from mammals and nonmammals separately and then analyzed the networks of covarying residues from the perspective of function. Although H2 and H3 are structurally similar, the differences in the degrees of frustration in parts of H2 and H3 result in these regions being the likely initiation sites for the $PrP^C \rightarrow PrP^{SC}$ transition in mammalian prions.

The conclusions reached from the sequence-based SCA are complemented by probing the response of mouse ($mPrP^C$) and human PrP^C ($huPrP^C$) to mechanical force without and with a disulfide (SS) bond between Cys179 and Cys214. By generating a number of unfolding trajectories, we generated a free energy profile, $G(R)$, as a function of molecular extension R. The profile and the dynamics of rupture of contacts clearly delineate the order of unfolding. The instability associated with residues in H2 and H3 results in their unfolding prior to the more stable parts. Although there are differences in the mechanical stability of PrP^C under reducing conditions (no SS bond) and oxidizing conditions (SS bond intact), the initial unfolding, which is needed to access PrP^{C*}, is localized in H2 and H3. Both the evolutionarily based analysis and responses to mechanical force show that the initial transition in the conversion from the cellular form to the scrapie form must involve conformational changes in C-terminal helices H2 and H3. The results of SCA also explain the absence of PrP^{SC} formation in nonmammals.

METHODS

Statistical Coupling Analysis. To identify the network of residues that are evolutionarily related, we use our formulation[22,23] of the sequence-based statistical coupling analysis (SCA) introduced by Lockless and Ranganathan in their pioneering studies.[19−21] SCA is remarkably versatile and provides physically meaningful results provided the database of sequences is large.[24] We first created a multiple-sequence alignment of the PrP^C sequences. A statistical free energy-like function at each position, i, in a multiple-sequence alignment (MSA) is defined as

$$\frac{\Delta G_i}{k_B T^*} = \sqrt{\frac{1}{C_i}\sum_{x=1}^{20}\left[p_i^x \ln\left(\frac{p_i^x}{p_x}\right)\right]^2} \quad (1)$$

where $k_B T^*$ is an arbitrary energy unit, C_i is the number of types of amino acids that appear at position i, and p_x is the mean frequency of amino acid x in the MSA. In eq 1, $p_i^x = n_i^x/N_i$, where n_i^x is the number of times amino acid x appears at position i in the MSA and $N_i = \sum_{x=1}^{20} n_i^x$.

The basic hypothesis of the SCA is that correlation or covariation between two positions i and j may be inferred by comparing the statistical properties of the MSA and a subalignment of sequences (derived from the MSA) in which a given amino acid at position j is conserved ($S_j = 0$). The restriction that $S_j = -\sum_{x=1}^{20} p_j^x \ln p_j^x = 0$ in the subalignment is termed sequence perturbation at position j.[19] The effect of perturbation is assessed using

$$\frac{\Delta\Delta G_{ij}}{kT^*} = \sqrt{\frac{1}{C_i}\sum_{x=1}^{20}\left[p_{i,j}^x \ln\left(\frac{p_{i,j}^x}{p_x}\right) - p_i^x \ln\left(\frac{p_i^x}{p_x}\right)\right]^2} \quad (2)$$

where $p_{i,j}^x = n_{i,j}^x/N_{i,j}$, $n_{i,j}^x$ and $N_{i,j}$ are the number of sequences in the subalignment in which x appears in the ith position, and $N_{i,j} = \sum_{x=1}^{20} n_{i,j}^x$. The coupling between sites i and j inferred using eq 2 differs from the original formulation, which has little consequence with respect to the qualitative conclusions.[25] Our procedure, which is a generalization of sequence entropy,

dx.doi.org/10.1021/bi3005472 | Biochemistry 2013, 52, 310−319

has been successfully used to identify an allostery wiring diagram in enzymes.[23]

To obtain statistically meaningful results using the SCA, it is important to choose the subalignments appropriately.[25] Let $f = p/N_{MSA}$, where p is the number of sequences in the subalignment and N_{MSA} is the total number of sequences in the MSA. We set f equal to 0.35 to satisfy the central limit theorem,[25] ensuring that the statistical properties of the subalignments coincide with those of the full MSA. Using an f of 0.35, we calculated matrix elements $\Delta\Delta G_{ij}$ that estimate the response of position i in the MSA to all allowed perturbations at j ($S_j = 0$). The rows (labeled i) in $\Delta\Delta G_{ij}$ correspond to positions in the MSA. We determined the network of covarying residues using elements $\Delta\Delta G_{ij}$ in conjunction with the coupled two-way clustering algorithm.[26] The extent to which rows $\Delta\Delta G_{ij}$ and $\Delta\Delta G_{kj}$ are similar is assessed using the Euclidean measure.[25] Because $\Delta\Delta G_{ij} = 0$ for perfectly conserved positions and for sites where the amino acids are found at their mean frequencies in the MSA ($p_i^x = p_i$), the SCA cannot predict the role these residues might play in the function or dynamics of the enzyme.

Self-Organized Polymer (SOP) Model for Prion Protein. To study the instabilities in the ordered regions of PrP^C, we simulated the effect of mechanical force using the coarse-grained self-organized polymer (SOP) model, which has been used with considerable success in predicting the outcomes of single-molecule force spectroscopy of proteins and RNA[27−29] as well as in describing complex dynamical processes ranging from protein folding to allosteric transitions in proteins.[23,30,31] Because force does not alter the interactions involving the protein of interest, the response of proteins to force is particularly well suited to probing specific regions of instability. In the simplest version of the SOP model, the structure of a protein is represented using only the C_α coordinates, r_i (i = 1, 2, ..., N), with N being the number of amino acids. The potential energy of the prion protein in the SOP representation is

$$\begin{aligned} H(\{r_i\}) &= V_{FENE} + V_{NB}^{ATT} + V_{NB}^{REP} \\ &= -\sum_{i=1}^{N} \frac{k}{2} R_0^2 \log\left[1 - \frac{(r_{i,i+1} - r_{i,i+1}^0)^2}{R_0^2}\right] \\ &\quad + \sum_{i=1}^{N-3} \sum_{j=i+3}^{N} \varepsilon_h \left[\left(\frac{r_{ij}^0}{r_{ij}}\right)^{12} - 2\left(\frac{r_{ij}^0}{r_{ij}}\right)^{6}\right]\Delta_{ij} \\ &\quad + \left[\sum_{i=1}^{N-2} \varepsilon_l \left(\frac{r_{i,i+2}^0}{r_{i,i+2}}\right)^{6} + \sum_{i<j} \varepsilon_l \left(\frac{\sigma}{r_{ij}}\right)^{6} (1 - \Delta_{ij})\right] \end{aligned} \tag{3}$$

where the distance between two adjacent α-carbon atoms is $r_{i,i+1}$, $r_{i,j}$ is the distance between the ith and jth α-carbon atoms, and $r_{i,j}^0$ is the corresponding distance between the ith and jth α-carbon atoms in the folded structure. The first term in eq 3, the finite extensible nonlinear elastic (FENE) potential, accounts for chain connectivity. The stability of the protein is described by the nonbonded interactions (the second term in eq 3) that assigns attractive interaction between two residues that are in contact in the native structure. Nonbonded interactions between residues that are not in contact in the native structure are taken to be purely repulsive (the third term in eq 3). The value of $\Delta_{i,j}$ is 1 if i and j are in contact in the native structure and is zero otherwise. A native contact implies that the distance between the ith and jth interaction centers is less than a cutoff distance R_C (0.8 nm in this study).

The spring constant, k, in the FENE potential (the first term in eq 3) for stretching a covalent bond is 2000 kcal mol^{-1} nm^{-2}, and the value of R_0, which gives the allowed extension of the covalent bond, is 0.2 nm. The values of parameters ε_h, ε_l, and σ are taken to be 1.2 kcal/mol, 1.0 kcal/mol, and 0.38 nm, respectively. Because there are only a few parameters in the SOP energy function, we can exhaustively explore the physical processes governing the unfolding of prion protein under tension.

Simulations. We assume that the dynamics of the system can be described using the Langevin equation in the overdamped limit. The equation of motion for the ith α-carbon atom is given by

$$-\zeta \frac{\partial \vec{r}_i}{\partial t} = -\frac{\partial H(r_i)}{\partial \vec{r}_i} + \vec{\Gamma}_i(t) \tag{4}$$

where ζ is the friction coefficient and $\Gamma_i(t)$ is a random force with a white noise spectrum. We start the Brownian dynamics simulations by first equilibrating the prion protein at 300 K. Subsequently, an external force is applied to the C-terminal end of the prion protein while the N-terminus is fixed. By symmetry, the direction of pulling does not affect the calculation of scalar quantities. In the constant loading rate simulations, force is continuously increased by attaching a spring [mimicking the harmonic trap in a laser optical tweezer experiment (LOT) or a cantilever in AFM experiments] with a spring constant k_s of 0.15 pN/nm. Thus, the effect of applying force to the C-terminus of the protein leads to an external mechanical force $f(t) = -k_s(z_c^0 - v_s t)$, where z_c^0 is the initial position of the C-terminal α-carbon atom and v_s is the pulling velocity. We use a v_s of 6.4×10^3 nm/s and a k_s of 0.15 pN/nm. Thus, loading rate $r_f = k_s v_s$ = 960 pN/s, which is comparable to the range used in typical AFM experiments but is approximately 5−100 times larger than the values in LOT experiments.

We estimate the time scale involved in the unfolding of prion protein using typical values of the friction coefficient (eq 4) and energy scale in the SOP energy function (eq 3), which yields $\tau_H \approx [(\zeta_H \varepsilon_h)/(k_B T_s)](\tau_L)^2$. For our choice of parameters, we obtain τ_L = 4 ps[23,31,32] with ε_h = 1.2 kcal/mol, $\zeta_H = 100/\tau_L$, and T_s = 300 K. Integration time step $h = 0.05\tau_H$, and using the natural measure of time for the overdamped condition for τ_H gives h = 40 ps.

Fraction of Contacts. To describe the order of unfolding of various structural elements of PrP^C upon the application of force, we calculated the time-dependent fraction of contacts between secondary structures, which is defined as $f_C(t) = [\sum_{i=1,L} N_C^i(t)/N^o]/M$, where i is the index of the trajectory, M is the total number of trajectories, and $N_C^i(t)$ and N^o are the number of native contacts in the ith trajectory at time t and the number of native contacts in the crystal structure, respectively. We calculated $f_C(t)$ for the $\beta1-\beta2$, $\beta2-$H2, $\beta2-$H3, and H2−H3 groups. In addition, we also calculated $f_C(t)$ for the three helices.

Energy Landscape. The free energy profile as a function of end-to-end distance R is calculated using $G(R) = -k_B T \log[P(R)]$, where $P(R)$ is the normalized probability of R over a total number of M (M is 200 in our case) trajectories. At a constant loading rate, the extension of the protein R increases (decreases) with an increasing (decreasing) pulling force f. We

dx.doi.org/10.1021/bi3005472 | Biochemistry 2013, 52, 310−319

count, for each of the M trajectories, the number of conformations, $N^i(R)$, with a certain value of R where $i = 1-M$. We calculate $P(R) = (1/M)\sum_{i=1}^{M} N^i(R)$, from which $G(R)$ is readily obtained. Because the calculations are performed at a constant loading rate, the calculated $G(R)$ does not represent an equilibrium free energy profile. The free energy profile together with the dynamics of loss of structure provides information about the order of unfolding of the secondary structural elements and hence provides quantitative information about the regions of instability.

RESULTS

To obtain a multiple-sequence alignment (MSA) for mammals and nonmammals, we first searched the nonredundant protein sequence database using PSI-BLAST. For mammals, the prion protein sequence from *Mus musculus* (mouse) is used as a query sequence and only mammalian sequences are searched. In all, 454 sequences are obtained after convergence (additional rounds of iterations in PSI-BLAST yield no new sequences) for mammals. Similarly, the *Trionyx sinensis* (Chinese soft shell turtle) sequence is used to identify the nonmammalian sequences, and 43 sequences are saved after convergence. We manually curated the sequences to eliminate those that are too long or too short and contain large gaps in the MSA. The resulting sequences were aligned using ClustalW.[33] With this procedure, our MSA consists of 342 sequences for mammalian PrP^C and only 21 sequences for nonmammalian prions. The small number in the MSA for nonmammalian prions does add uncertainty to the analysis of nonmammalian prions. However, given the stark differences in the SCA predictions between nonmammals and mammals, we believe that the qualitative conclusions should be robust.

Residues in the Signal Domain Correlate More with Other Regions of PrP^C in Mammals Than in Nonmammals. The clustered residues, obtained using the SCA, are shown in Table 1 for mammalian and nonmammalian prion proteins. The identities and positions of the amino acids in the network of covarying residues are labeled according to their positions in mouse PrP^C (Figure 2). In mammals, the clustered N-terminal residues, Met1, Ala2, Asn3, Leu4, Tyr6, Leu8, Met15, and Val19, are part of the endoplasmic reticulum targeting the signal peptide that directs the post-translational transport of prion protein into the plasma membrane.[17] In contrast, there is only one residue, Lys24, located in the cleavage site that is involved in the signal domain for nonmammalian prion proteins (see Table 1). We surmise that the signal domain in nonmammals is not as conserved as it is in the mammalian counterpart. These differences suggest that mammalian and nonmammalian prions could have different cellular functions.

Table 1. Networks of Residues in Mammalian and Nonmammalian Prion Proteins

	residue indices as in mouse prion protein
mammals	1, 2, 3, 4, 6, 8, 15, 19, 94, 96, 111[a]
	137, 165, 183, 202, 204, 218, 219, 226, 227, 231, 233, 234[b]
nonmammals	24, 29, 37, 49, 100, 103, 106, 107, 109, 112, 115, 116, 117, 119, 120, 121[a]
	134, 152, 155, 158, 160, 175, 180, 208, 217[b]

[a]Disordered NMR structure. [b]Ordered NMR structure.

Mammalian Sequences Are More Conserved in the Redox-Related Region Than Sequences from Nonmammalian PrP^C. In mammals, residues Thr94, Asn96, and Val111, neighbors of residue His95 or His110, are highly correlated with the residues in the octarepeat region of the unstructured, highly flexible N-terminus that is asserted to bind copper. In contrast, in nonmammals, only one residue, Lys109, is included in the cluster (Table 1). These differences are also reflected in the differences in sequence between mammalian and nonmammalian prion proteins in this region (Figure 2b). For example, mammalian PrP^C contains a number of Gly residues, whereas in nonmammalian prion proteins, there are fewer Gly residues. In addition, there are greater variations in this region in nonmammalian prions than in mammalian PrP^C. It is unclear if the highly conserved region, which is structurally disordered, plays any significant role in the conversion process. The reduced flexibility in nonmammalian PrP^C tidily explains the observation that the structure of the N-terminal region of nonmammalian PrP^C is stable and protease-resistant and does not bind copper.[17] The differing behavior of mammalian and nonmammalian prion proteins, with regard to the copper-binding related redox reaction, supports the hypothesis that copper binding may not be the primary function of prion protein.[34] We cannot rule out the possibility that the emergence of prion disease is related to the metal-induced redox reaction,[35,36] which has been suggested as a common mechanism in initiating both Alzheimer's disease and prion disorders.

It has been suggested that the presence of the GxxxG transmembrane binding motifs (Figure 2) in mammalian prions in the region of residues 110−130 covering M128 is essential in triggering prion disorders. Here, we find that the GxxxG motifs are also present in nonmammalian prions (see Figure 2) in the same region. In mammalian prions, M128 is highly conserved, whereas it is less so in nonmammlian prions (Figure 2). The similarities in the properties of the sequences in this region between mammals and nonmammals suggest that this region may not encode the initiating sites in the $PrP^C \rightarrow PrP^*$ transition. However, it is well-known that a common polymorphism at this position in $huPrP^C$ has a strong influence on the kinetics of fibril formation[37] even though this behavior is exhibited very little at the monomer level. For example, polymorphism does not alter the efficiency of conversion from the cellular form to PrP*. The differences are evident only in the formation of the critical nucleus and beyond.[37] Thus, although polymorphism may not influence the earliest transitions, clearly they affect the kinetics of fibril formation, which is beyond the scope of this study.

In addition to the difference described above, Table 1 also shows that residues Lys100, Lys103, Thr106, Asn107, Lys109, Ala112, Ala115, Ala116, Ala117, Ala119, Val120, and Val121 are not clustered in mammals. Indeed, these residues are highly conserved in mammals and do not covary with other regions of the prion proteins (Figure 2b). On the other hand, in nonmammals, these residues are evolutionarily related (Table 1). Finally, residues in H2 and H3 are conserved to a greater extent in mammals than in nonmammals (Figure 2c). In addition, the stretch of TTTT in H2 is rare and is highly conserved in mammalian prions. This pattern of T residues has a great propensity to be in a β-strand conformation in a majority of proteins.[15] However, they are part of a helix in mammalian PrP^C, thus making it unusual. Taken together, these results suggest that several residues in H2 and H3 are frustrated

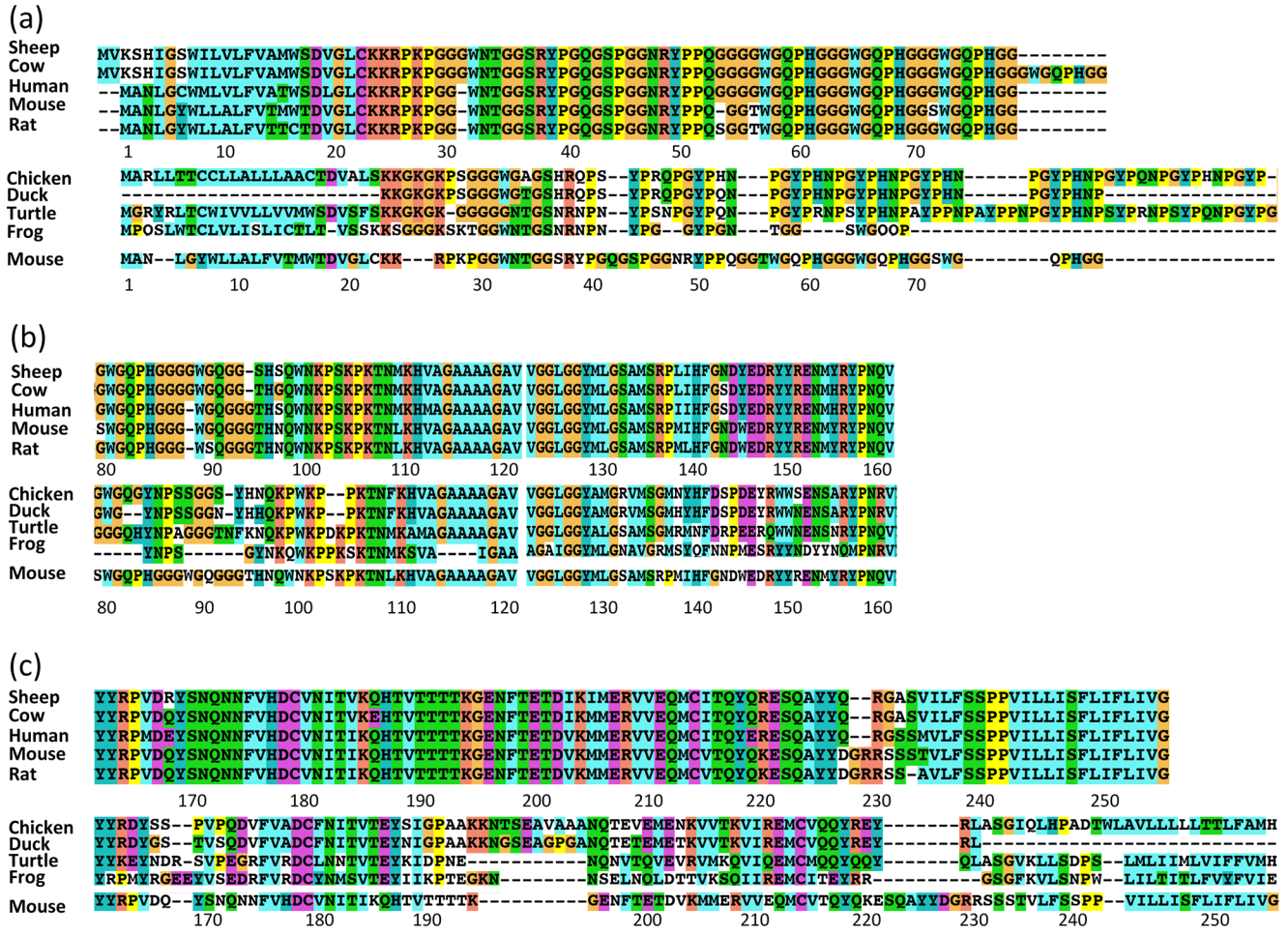

Figure 2. Alignment of sequences of prion proteins from mammals and nonmammals. The numbering of residues is that of $mPrP^C$. The sequence of $mPrP^C$ is listed at the bottom of the group of nonmammals. To display the alignment clearly, we split the sequence into three parts. (a) We show the alignment of residues 1−79. (b) Residues 80−160 are shown. (c) Residues 161−254 are shown.

in a helical state and hence are likely to be part of the initiating sites in the $PrP^C \rightarrow PrP^*$ transition.

Clustered Residues in the C-Terminus Are Delocalized in Mammals but Form Stable Localized Interactions in Nonmammals. The NMR structure in Figure 1 (PDB entry 1AG2) shows that the C-terminus of PrP^C has three α-helices and a two-stranded antiparallel β-sheet.[5,38] Covarying residues in the network of mammals and nonmammals are shown with spheres on the same structure for comparison (green for residues clustered in mammals and red for nonmammals). Clearly, all the red spheres are localized near the center of mass of the protein. The residues that are colored green are distributed in the peripheral region (the cartoon representation of the protein chain is colored according to their distance from the center of mass, with red being the closest and the blue being the farthest). It appears that the residues in the center of nonmammalian prion protein are evolutionarily related to maintain a stable structure. We conclude that these residues are not frustrated and the corresponding sequences are concordant, implying that the α-helical secondary structures adopted by these residues are compatible with the theoretically predicted structures for these sequences.

Our previous studies predicted that as a result of instabilities in the dynamics of the helical fragments localized in the second half of H2 and parts of H3 they would undergo a transition from α-helical conformation to a β and/or random coil state[15,16] during the PrP^C to PrP^{SC} transition. This work shows that the clustered residues in nonmammalian sequences are located in the stable helical fragment (Asn152, Arg155, Val175, Asn180, and Val208). In contrast, for mammals, all the clustered helical residues are part of frustrated helices H2 and H3. For example, Ile183 is close to the second half of H2, and residues Val202, Met204, Glu218, Lys219, and Asp226 are part of H3. These results confirm the earlier predictions that the frustrated regions localized in H2 and H3 are most susceptible to conformational change and could be designated as initiation sites in the $PrP^C \rightarrow PrP^*$ transition. In contrast, we predict that H2 and H3 in PrP^C from *T. sinensis*, a nonmammalian species, are not as frustrated, thus explaining the lack of formation of PrP^{SC} in these species.

Forced Unfolding of $mPrP^C$ and $huPrP^C$ Starts from H3 and H2. To complement the predictions based on evolutionary imprints using the SCA, we also conducted Brownian dynamics simulations (see Methods) to unfold $mPrP^C$ and $huPrP^C$ using mechanical force. We first describe results for prion proteins without the disulfide bond. At a constant loading rate, $mPrP^C$ unfolds in two distinct steps (black trajectory in Figure 3a). When $f \approx 35$ pN, the molecular extension of the prion protein, R, increases by ∼10 nm. This step is associated with the rupture of H3 and H2. In the second step, when $f \approx 40$ pN, R increases from 15 to 20 nm and is

dx.doi.org/10.1021/bi3005472 | *Biochemistry* 2013, 52, 310−319

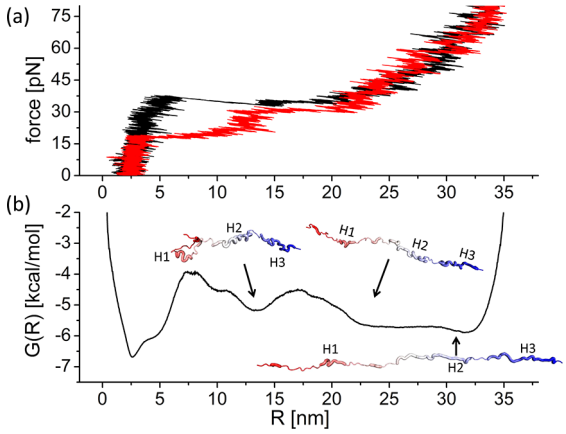

Figure 3. (a) Force−extension curves for two trajectories generated by pulling mPrP^C from the C-terminus while keeping the N-terminus fixed. The structures that unravel at various stages as force is increased are shown for the black trajectory. (b) Free energy-like profile generated using the histogram of extensions sampled in 100 pulling simulations. Representative conformations in the basin at $R \sim 14$ nm, $R \sim 23$ nm, and $R \sim 33$ nm are shown.

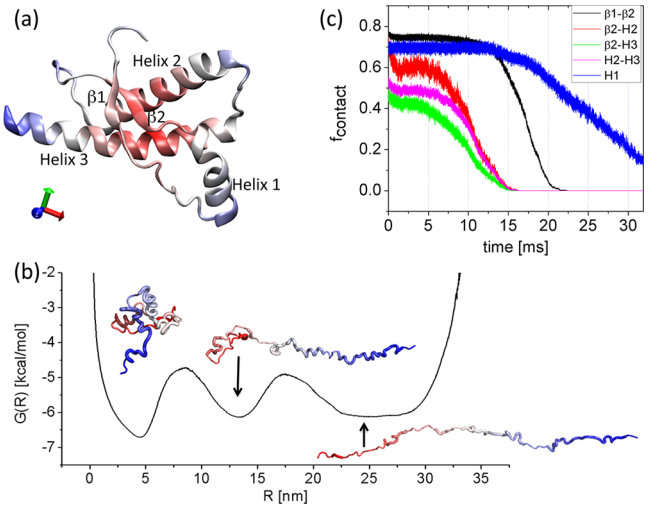

Figure 4. (a) Cartoon representation of the human prion protein (PDB entry 1QLX) displaying only the structured C-terminal region. The secondary structural elements are labeled. (b) Free energy profile, $G(R)$, generated using the histogram of extensions sampled in 100 pulling simulations. Representative conformations in the basin at $R \sim 5$ nm, $R \sim 13$ nm, and $R \sim 25$ nm are shown. (c) Time-dependent changes in the loss of fraction of contacts between different secondary structural elements labeled in the figure.

associated with unfolding of the two β-strands (Figure 1) and H1.

Using the force−extension curves from ∼100 unfolding trajectories, we calculated $G(R) = -k_BT \ln P(R)$, where $P(R)$ is the distribution of R. The free energy profile $G(R)$ (Figure 3b) shows that there are two major steps in the unfolding of PrP^C. When chain extension exceeds the distance between the folded state ($R = 2.3$ nm) to the first barrier that is ∼5 nm (Figure 3b) away, H3 and H2 unfold. By extrapolating the estimated barrier to unfolding obtained at roughly $f \sim 35$ pN to zero force using $G(R|f = 35\ \text{pN}) = G(R|f = 0) - \Delta Rf$), where $\Delta R = 5$ nm − 2.3 nm = 2.7 nm, we find that the barrier at $f = 0$ would be ≈19 kcal/mol, which is remarkably similar to that estimated in experiments.[14] The minimum at $R \sim 13$ nm corresponds to an intermediate state, which corresponds to conformations with H2 and H3 unfolded. The total number of residues in H2 and H3 is 48, which implies that at full extension the length gain due to their unfolding should result in $R \approx 18$ nm assuming an extension of $a \approx 0.38$ nm per amino acid. However, we find that when H2 and H3 rupture at $f \approx 35$ pN the gain in length is $R \approx 12$ nm, which implies that there is residual helical structure when these segments are stretched (see the conformations in Figure 3). Incomplete stretching has also been reported in other helical proteins.[39] The second barrier at $R \sim 18$ nm represents extension involving H1 and rupture of contacts between the two β-sheets in the N-terminus of the prion structure.

Force-induced unfolding results for huPrP^C (Figure 4a) obtained using the structure (PDB entry 1QLX) are shown in Figure 4. H3 in huPrP^C is longer than that in mPrP^C, which results in the R of the native state being longer than in mPrP^C. Taking this fact into account, we find that the calculated $G(R)$ profiles (compare Figures 3b and 4b) are similar. Just as in mPrP^C, when R exceeds the first barrier located ∼4.5 nm away from the folded state, H2 and H3 unfold and populate an intermediate state. Both profiles clearly show that unfolding occurs through an intermediate, at $R \sim 10$ nm from the folded state, in which interactions involving H2 and H3 are disrupted just as in mPrP^C. It is also interesting to note that sequence effects are manifested in the finer details of $G(R)$, indicating that single-molecule pulling experiments can be profitably used to tease out the differences between various prion proteins. Thus, the free energy profiles, including the barrier height separating the folded and intermediate states, are similar. These results are not surprising given that the structures of mPrP^C and huPrP^C are homologous.

Dynamics of Force-Induced Loss of Tertiary Interactions. The contact map for the ordered C-terminal portion of mPrP^C shows (Figure 5a) interactions between β1 and β2 as well those involving H2, H3, and β1 and β2. To assess the temporal loss of these contacts upon stretching, we calculated the time-dependent decrease in the fraction of contacts during the unfolding process (see Methods). At $t = 0$, the fraction of contacts $f_C(0)$ involving β2 and H3 is ≈0.5, meaning that almost half of the native contacts involving these elements are absent at room temperature. Similarly, for β2−H2 and H2−H3 contacts, $f_C(0) \approx 0.6$. The equilibrium value of $f_C(0)$ involving β1−β2 groups is ≈0.8. The time-dependent decrease in $f_C(t)$ involving these secondary structural elements upon the application of force is shown in Figure 5b. We find that the loss of contacts between H3 and the β2 occurs first (Figure 5b), followed by the rupture of the contacts between H3 and H2, and H2 and β2. Interactions between β1 and β2 at the N-terminus of the prion protein are the most stable and are disrupted only during the last stages of unfolding. Interestingly, the helical structure of H1 is relatively intact even after complete disruption of structure in the rest of the molecule. If the entire C-terminal region of PrP^C with 111 amino acids is fully extended, we expect $R \approx (N - 1)a \approx 42$ nm. However, we find that even at $f \approx 75$ pN, R falls short of 42 nm. Nearly full extension, realized only upon stretching of H1, occurs when $f \approx 120$ pN. This shows that H1, stabilized by salt bridges, is unlikely to undergo conformational changes in the early stages of the PrP^C → PrP^{SC} transition.

The dynamics of rupture of tertiary contacts in huPrP^C (Figure 4c) is nearly quantitatively identical to that observed in mPrP^C. Here, interactions involving H3 and H2 are disrupted

dx.doi.org/10.1021/bi3005472 | Biochemistry 2013, 52, 310−319

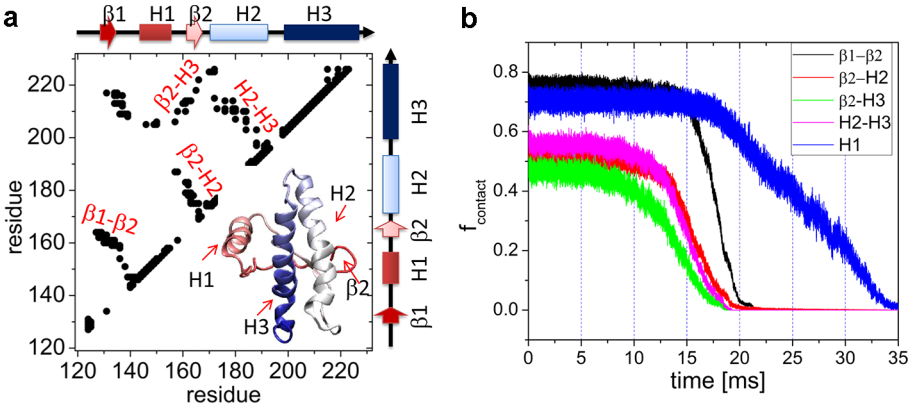

Figure 5. (a) Contact map of mPrP^C corresponding to the structure shown in Figure 1. Two residues are in contact if the distance between them is less than 0.8 nm. The contact map shows that H1 is peripherally located and does not form interactions with the rest of the ordered C-terminal residues. (b) Time-dependent changes in the loss of fraction of contacts between different secondary structural elements labeled in the figure. Remarkably, H1 resists mechanical force the most and is disrupted only after the loss of all the interactions in the rest of the protein.

prior to the rupture of contacts of β1, β2, and finally H1. Thus, on the basis of pulling simulations of mPrP^C and huPrP^C, we conclude that the major instabilities are localized in H2 and H3.

Forced Unfolding of mPrP^C with an Intact S−S Bond. Mammalian prions contain an internal disulfide bond between Cys179 and Cys214 that tethers H2 and H3 to each other (Figure 6a), thus enhancing the stability of the region around

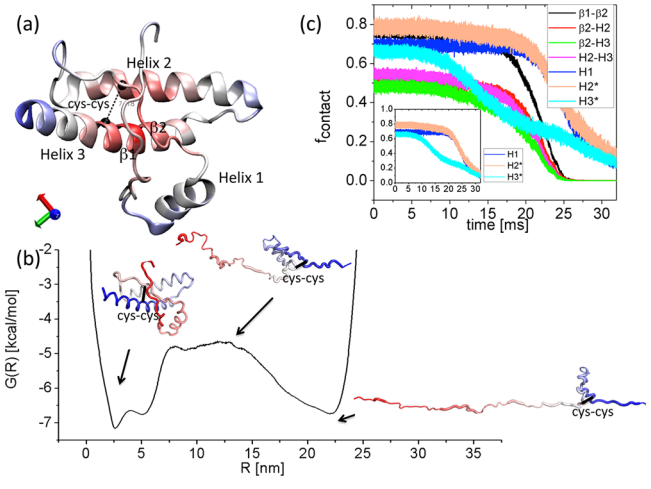

Figure 6. (a) Structured C-terminus of the mouse prion with the disulfide bond shown as a black dashed line. (b) Dependence of the free energy profile generated using the histogram of extensions sampled in 100 pulling simulations as a function of the molecular extension, R. Representative conformations in the basin at $R \sim 2.5$ nm, $R \sim 13$ nm, and $R \sim 23$ nm are shown. (c) Time-dependent changes in the loss of fraction of contacts between different secondary structural elements labeled in the figure. f_C values for H1, H2*, and H3* (see the text for definitions) are shown in the inset.

the S−S bond. We conducted Brownian dynamics simulations to assess the influence of f on the internal stability of mPrP^C with an S−S bond present. In these simulations, the covalent S−S bond is modeled by adding a stiff FENE potential (first term in eq 3) between Cys179 and Cys214 with a k of 2000 kcal mol^{-1} nm^{-2}.

Free energy profile $G(R)$ in Figure 6b shows that with an intact S−S bond the entire PrP structure is more stable, and the intermediate state at $R \sim 13$ nm found in mPrP^C is absent (compare Figures 2b and 5b). Because of the S−S bond restraint, the helical contents of H2 and H3 between Cys179 and Cys214 remain intact throughout the simulations. However, the helical structures outside the region surrounding the S−S bond are less stable and are the first to rupture. As shown in Figure 6c, in the early stage of pulling simulations (0−20 ms), the fraction of contacts in the first half of H2 (residues 171−179, denoted H2*) decreases. Residues in the second half of H3 (residues 214−223, labeled H3*) lose a large fraction of their contacts. In contrast, the fraction of contacts in H1 remains 0.7. Thus, there is a consistency in the extent of frustration in regions associated with H2 and H3 both with and without the S−S bond.

DISCUSSION

Although the structures of a number of species of PrP^C have been determined, the sequence of events that drive the monomer to scrapie form is not well understood. From analyses of both sequence and structure,[15] experiments,[40,41] molecular dynamics simulations,[16] and the response to mechanical force (Figures 3−6), it is clear that H1 is stable. In mammalian prions, the stability arises because of the perfect placement of oppositely charged residues at locations i and i + 4.[16] Such an arrangement is rarely, if ever, found in proteins in the genomes of *Escherichia coli* and yeast genomes.[16] More importantly, experiments using CD and NMR[42,43] show that isolated H1 is extremely stable with a high degree of helical content over a wide range of solvent conditions. Using helical constructs from mPrP^C, with a few flanking residues that apparently do not have any influence on the helix population of the interior residues, it was demonstrated[42] that H1 has a strong intrinsic helix propensity. A later study[43] probed the stability of isolated H1 from huPrP^C over a broad range of solution conditions. Surprisingly, the intrinsic helical content is nearly 60%, which is unusual given that there are no long-range tertiary interactions to stabilize the isolated H1. Both these studies[42,43] assert that H1 is unlikely to be involved in the conversion to the scrapie form, with the latter[43] emphasizing that the stability of H1 could be a barrier in the PrP^C → PrP* transition. These observations suggest that, at least in the early stages, it is unlikely H1 would undergo conformational changes. It should be noted that others have proposed a key role for H1 in initiating the PrP^C to PrP^{SC} conversion.[44,45] Our findings and

dx.doi.org/10.1021/bi3005472 | *Biochemistry* 2013, 52, 310−319

several experiments (see below) strongly suggest that the conformational change in stable H1 is not the dominant feature in the creation of the aggregation-prone PrP* from PrP^C. This conclusion does not imply that H1 does not undergo a change in conformation at later stages. However, such a possibility has been ruled out in certain recent experiments.[11,40]

Experimental Evidence from Monomer Dynamics. The finding that the initiation sites that drive the $PrP^C \rightarrow$ PrP* transition must involve helices H2 and H3 finds considerable experimental support. Several experiments, probing the dynamics of mammalian PrP^C and their mutants, under a variety of conditions have established that H2 and H3 undergo substantially larger fluctuations than the rest of the structure and thus point to their potential instability.[46−48] (1) Perhaps the earliest evidence for the potential role that H2 and H3 play in creating PrP* in Syrian hamster comes from the $^{15}N-^{1}H$ two-dimensional NMR experiments,[41] which showed that in a small population of the aggregation species H2 and H3 are locally disordered. They further suggest that the transition to the PrP* state, with disordered H2 and H3, may be the key step in the association with the scrapie form. (2) More recently, Bae et al.[47] have used NMR to characterize the intrinsic flexibility of $mPrP^C$ and a few key mutants. By measuring the NMR order parameters, they surmise that regions of H2 and H3 have smaller values of the order parameter and hence are more flexible (see the discussion related to Figure 4 in ref 47). On the basis of this study, they assert that segments that span H2 and H3 may constitute the initiating sites for pathogenic mutants as well as the wild type. It is worth noting that amino acid sequences in the C-terminal mammalian prions are well conserved,[49] which implies that the initiation sites for the $PrP^C \rightarrow$ PrP* transition are likely to be similar in all mammalian species. (3) It has been argued that β-PrP^C, an intermediate lacking an S−S bond created under acidic conditions, has enhanced β-strand content.[50] In this conformation, H2 is apparently unstable, whereas there is helical content in H3. This study is not inconsistent with our conclusions. As already noted in ref 50, the presence of structure in H3 given that H2 is unstable is puzzling especially considering that β-PrP^C has far greater α-helical content than the conformations adopted in the fibrils. Furthermore, the monomers in the fibril have a parallel in-register β-sheet arrangement involving both H2 and H3 (see below). Nevertheless, the stability of H1 and the instability of H2 in β-PrP are consistent with our findings. (4) Finally, analyses of dynamics of structural domains based on short molecular dynamics simulations[51] have argued that H3 is unstable, which is consistent with our study. However, they also suggest that H1 is dynamically unstable, which is not supported by this study or by experiments showing that even the isolated H1 is stable.[42,43] More recently, Santo et al.[52] have shown using computations and NMR experiments with a number of mammalian prions that the largest dynamical domain is localized in H2 and H3. In addition, the dynamics associated with this region is coupled to β2 just as found in this study (see Figures 3c and 4c). It is gratifying that a number of different approaches yield a consistent picture of the role of H2 and H3 in the initial stages of the $PrP^C \rightarrow$ PrP* transition. As shown here, fluctuations in this region arise due to decreased stability, which in turn can be traced to the unusual sequence composition of H2.[15] Not coincidentally, many of the naturally occurring pathogenic mutations are also found here.

Destabilization of H2 and H3, which form the substantial core of PrP^C, could result in unfolding of the whole protein. As a result of nearly global unfolding, most of the prion protein would be exposed to the solvent. Results from two NMR experiments could be used to infer that all three helices have similar stabilities based on their dynamical behavior. (a) Equilibrium H−D exchange experiments with $huPrP^C$ conducted some time ago[53] found that the protection factor for the core of the protein was essentially the same as the equilibrium constant between the folded and unfolded states. However, from these equilibrium experiments, the order of unfolding in individual molecules cannot be deduced nor can the population (estimated to be ∼1%)[41] of PrP* molecules be inferred. The initial disruption of structures associated with H2 and H3 ensures that interactions associated with H1 are destabilized rapidly, thus explaining the observed pattern of protein factors.[53] (b) It has been suggested[54] that for truncated $mPrP^C$ (residues 113−231) all three helices have similar flexibility. Although the results of this study are not in agreement with the conclusions reached elsewhere,[47] even these authors identify regions of H2 as potential initiation sites.

Consistency with Proposed Fibril Structures. Recent experiments provide convincing evidence that in the fibril state H2 and H3 have altered conformations and adopt β-strand structures. (1) Using H−D exchange experiments with PrP^{SC} formed from $huPrP^C$, it was established that the highest protection factors were found in residues starting around position 169 and encompassing H2 and H3.[40] They attributed the large values of the protection factor to extended hydrogen-bonded cross-β structure. In a subsequent study, Surewicz and co-workers[10] used site-directed labeling and EPR to demonstrate that in the fibril state the core of the protein (including H2 and H3) forms single-layer structures that are stacked in an in-register parallel manner. (2) More recently, constraints obtained from solid state NMR experiments with Syrian hamsters provided compelling evidence that the fibril core is formed from residues 173−224, which includes H2 and H3. These segments form β-strands. These experiments and the high β-strand content of PrP^{SC} cannot be explained without invoking a critical role for H2 and H3 in the conversion process. We conclude that our results are consistent with a substantial number of experiments with both monomers and fibrils.

■ CONCLUSIONS

Our findings and experiments cited above show that frustrated helices H2 and H3 must undergo a transition to an assembly competent state, PrP*, by adopting an extended strand conformation. It should be emphasized that we are referring to instabilities associated with H2 and H3, which cannot be inferred from equilibrium titration of PrP^C in the presence of denaturants. Because such a transition involves nearly global unfolding of a substantial part of the protein (resulting in similar protection factors in the ordered regions of the equilibrium H−D exchange experiments[53]), the barrier separating PrP^C and PrP* must be large[13] so that under normal conditions the population of PrP* is likely to be small. This proposal is consistent with the finding that even at high pressures only ∼1% of the protein is in the PrP* state.[41] In addition, as PrP* molecules associate and grow, the strands resulting from the $\alpha \rightarrow \beta$ transition in H2 and H3 would form the core of the fibril as shown in a number of recent studies.[10,11,40,55] The resulting model, which favors formation of parallel β-strand fibrils involving conformationally altered H2 and H3 in the core, explains a number of biophysical

experiments, including the observation of high protection factors in the H−D exchange experiments in the core of the fibril.[40] Thus, despite the suggestion that PrP^{SC} could be described using β-helix[56] or β-spiral models[57] in which the C-terminal structures are intact (do not undergo conformational changes during the transition to the PrP^{SC} form), a majority of the recent experiments suggest a major role for H2 and H3 in initiation, as suggested here. We should emphasize, however, that a structural model of PrP^{SC} will be needed to establish the conformational changes in PrP^{C} that drive the cellular form to the pathogenic scrapie state.

AUTHOR INFORMATION

Corresponding Author

*Phone: (301) 405-4803. Fax: (301) 314-9404. E-mail: thirum@umd.edu.

Funding

We thank the National Science Foundation (CHE 09-4033) and the National Institutes of Health (GM089685) for supporting this work.

Notes

The authors declare no competing financial interest.

REFERENCES

(1) Prusiner, S. B. (1998) Prions. *Proc. Natl. Acad. Sci. U.S.A. 95*, 13363−13383.

(2) Aguzzi, A., and O'Connor, T. (2010) Protein aggregation diseases: Pathogenicity and therapeutic perspectives. *Nat. Rev. Drug Discovery 9*, 237−248.

(3) Legname, G., Baskakov, I., Nguyen, H., Riesner, D., Cohen, F., DeArmond, S., and Prusiner, S. (2004) Synthetic mammalian prions. *Science 305*, 673−676.

(4) Griffith, J. (1967) Self-replication and scrapie. *Nature 215*, 1043−1044.

(5) Riek, R., Hornemann, S., Wider, G., Billeter, M., Glockshuber, R., and Wuthrich, K. (1996) NMR structure of the mouse prion protein domain PrP(121−231). *Nature 382*, 180−182.

(6) Zahn, R., Liu, A., Luhrs, T., Riek, R., von Schroetter, C., Garcia, F., Billeter, M., Calzolai, L., Wider, G., and Wuthrich, K. (2000) NMR solution structure of the human prion protein. *Proc. Natl. Acad. Sci. U.S.A. 97*, 145−150.

(7) Calzolai, L., Lysek, D., Perez, D., Guntert, P., and Wuthrich, K. (2005) Prion protein NMR structures of chickens, turtles, and frogs. *Proc. Natl. Acad. Sci. U.S.A. 102*, 651−655.

(8) Glockshuber, R., Hornemann, S., Riek, R., Wider, G., Billeter, M., and Wuthrich, K. (1997) Three-dimensional NMR structure of a self-folding domain of the prion protein PrP(121−231). *Trends Biochem. Sci. 22*, 241−242.

(9) Diaz-Espinoza, R., and Soto, C. (2012) High-resolution structure of infectious prion protein: The final frontier. *Nat. Struct. Mol. Biol. 19*, 370−377.

(10) Cobb, N. J., Soennichsen, F. D., Mchaourab, H., and Surewicz, W. K. (2007) Molecular architecture of human prion protein amyloid: A parallel, in-register β-structure. *Proc. Natl. Acad. Sci. U.S.A. 104*, 18946−18951.

(11) Tycko, R., Savtchenko, R., Ostapchenko, V. G., Makarava, N., and Baskakov, I. V. (2010) The α-Helical C-Terminal Domain of Full-Length Recombinant PrP Converts to an In-Register Parallel β-Sheet Structure in PrP Fibrils: Evidence from Solid State Nuclear Magnetic Resonance. *Biochemistry 49*, 9488−9497.

(12) Tarus, B., Straub, J. E., and Thirumalai, D. (2006) Dynamics of Asp23-Lys28 salt-bridge formation in Aβ(10−35) monomers. *J. Am. Chem. Soc. 128*, 16159−16168.

(13) Thirumalai, D., Klimov, D. K., and Dima, R. I. (2003) Emerging ideas on the molecular basis of protein and peptide aggregation. *Curr. Opin. Struct. Biol. 13*, 146−159.

(14) Baskakov, I., Legname, G., Prusiner, S., and Cohen, F. (2001) Folding of prion protein to its native α-helical conformation is under kinetic control. *J. Biol. Chem. 276*, 19687−19690.

(15) Dima, R. I., and Thirumalai, D. (2002) Exploring the propensities of helices in prp^{c} to form β sheet using NMR structures and sequence alignments. *Biophys. J. 83*, 1268−1280.

(16) Dima, R. I., and Thirumalai, D. (2004) Probing the instabilities in the dynamics of helical fragments from mouse prp^{c}. *Proc. Natl. Acad. Sci. U.S.A. 101*, 15335−15340.

(17) Simonic, T., Duga, S., Strumbo, B., Asselta, R., Ceciliani, F., and Ronchi, S. (2000) cDNA cloning of turtle prion protein. *FEBS Lett. 469*, 33−38.

(18) Kallberg, Y., Gustafsson, M., Persson, B., Thyberg, J., and Johansson, J. (2001) Prediction of amyloid fibril-forming proteins. *J. Biol. Chem. 276*, 1294512950.

(19) Suel, G. M., Lockless, S. W., Wall, M. A., and Ranganathan, R. (2003) Evolutionarily conserved networks of residues mediate allosteric communication in proteins. *Nat. Struct. Biol. 10*, 59−69.

(20) Hatley, M. E., Lockless, S. W., Gibson, S. K., Gilman, A. G., and Ranganathan, R. (2003) Allosteric determinants in guanine nucleotide-binding proteins. *Proc. Natl. Acad. Sci. U.S.A. 100*, 14445−14450.

(21) Shulman, A. I., Larson, C., Mangelsdorf, D. J., and Ranganathan, R. (2004) Structural determinants of allosteric ligand activation in rxr heterodimers. *Cell 116*, 417−429.

(22) Dima, R. I., and Thirumalai, D. (2002) Exploring protein aggregation and self-propagation using lattice models: Phase diagram and kinetics. *Protein Sci. 11*, 1036−1049.

(23) Chen, J., Dima, R. I., and Thirumalai, D. (2007) Allosteric communication in dihydrofolate reductase: Signaling network and pathways for closed to occluded transition and back. *J. Mol. Biol. 374*, 250−266.

(24) Liu, Z., Chen, J., and Thirumalai, D. (2009) On the accuracy of inferring energetic coupling between distant sites in protein families from evolutionary imprints: Illustrations using lattice model. *Proteins: Struct., Funct., Bioinf. 77*, 823−831.

(25) Dima, R. I., and Thirumalai, D. (2006) Determination of network of residues that regulate allostery in protein families using sequence analysis. *Protein Sci. 15*, 258−268.

(26) Getz, G., Levine, E., and Domany, E. (2000) Coupled two-way clustering analysis of gene microarray data. *Proc. Natl. Acad. Sci. U.S.A. 97*, 12079−12084.

(27) Mickler, M., Dima, R. I., Dietz, H., Hyeon, C., Thirumalai, D., and Rief, M. (2007) Revealing the bifurcation in the unfolding pathways of GFP by using single-molecule experiments and simulations. *Proc. Natl. Acad. Sci. U.S.A. 104*, 20268−20273.

(28) Hyeon, C., and Thirumalai, D. (2007) Mechanical unfolding of RNA: From hairpins to structures with internal multiloops. *Biophys. J. 92*, 731−743.

(29) Lin, J.-C., and Thirumalai, D. (2008) Relative stability of helices determines the folding landscape of adenine riboswitch aptamers. *J. Am. Chem. Soc. 130*, 14080−14081.

(30) Hyeon, C., Dima, R. I., and Thirumalai, D. (2006) Pathways and kinetic barriers in mechanical unfolding and refolding of RNA and proteins. *Structure 14*, 1633−1645.

(31) Hyeon, C., Lorimer, G. H., and Thirumalai, D. (2006) Dynamics of allosteric transitions in GroEL. *Proc. Natl. Acad. Sci. U.S.A. 103*, 18939−18944.

(32) Veitshans, T., Klimov, D., and Thirumalai, D. (1997) Protein folding kinetics: Timescales, pathways and energy landscapes in terms of sequence-dependent properties. *Folding Des. 2*, 1−22.

(33) Chenna, R., Sugawara, H., Koike, T., Lopez, R., Gibson, T. J., Higgins, D. G., and Thompson, J. D. (2003) Multiple sequence alignment with the clustal series of programs. *Nucleic Acids Res. 31*, 3497−3500.

(34) Marcotte, E. M., and Eisenberg, D. (1999) Chicken prion tandem repeats form a stable, protease-resistant domain. *Biochemistry 38*, 667−676.

(35) Barnham, K. J., Cappai, R., Beyreuther, K., Masters, C. L., and Hill, A. F. (2006) Delineating common molecular mechanisms in Alzheimer's and prion diseases. *Trends Biochem. Sci. 31*, 465−472.
(36) Ji, H. F., Zhang, H. Y., and Chen, L. L. (2007) Why are prion diseases precluded by non-mammals? *Trends Biochem. Sci. 32*, 206−208.
(37) Lewis, P., Tattum, H., Jones, S., Bhelt, D., Batchelor, M., Clarke, A., Collinge, J., and Jackson, G. (2006) Codon 129 polymorphism of the human prion protein influences the kinetics of amyloid formation. *J. Gen. Virol. 87*, 2443−2449.
(38) Donne, D. G., Viles, J. H., Groth, D., Mehlhorn, I., James, T. L., Cohen, F. E., Prusiner, S. B., Wright, P. E., and Dyson, H. J. (1997) Structure of the recombinant full-length hamster prion protein prp(29−231): The N terminus is highly flexible. *Proc. Natl. Acad. Sci. U.S.A. 94*, 13452−13457.
(39) Gebhardt, J. C. M., Bornschloegla, T., and Rief, M. (2010) Full distance-resolved folding energy landscape of one single protein molecule. *Proc. Natl. Acad. Sci. U.S.A. 107*, 2013−2018.
(40) Lu, X., Wintrode, P. L., and Surewicz, W. K. (2007) β-Sheet core of human prion protein amyloid fibrils as determined by hydrogen/deuterium exchange. *Proc. Natl. Acad. Sci. U.S.A. 104*, 1510−1515.
(41) Kuwata, K., Li, H., Yamada, H., Legname, G., Prusiner, S., Akasaka, K., and James, T. (2002) Locally disordered conformer of the hamster prion protein: A crucial intermediate to PrP^{Sc}? *Biochemistry 41*, 12277−12283.
(42) Liu, A., Riek, P., Zahn, R., Hornemann, S., Glockshuber, R., and Wuthrich, K. (1999) Peptides and proteins in neurodegenerative disease: Helix propensity of a polypeptide containing helix 1 of the mouse prion protein studied by NMR and CD spectroscopy. *Biopolymers 51*, 145−152.
(43) Ziegler, J., Sticht, H., Marx, U., Muller, W., Rosch, P., and Schwarzinger, S. (2003) CD and NMR studies of prion protein (PrP) helix 1: Novel implications for its role in the PrPC → PrPSc conversion process. *J. Biol. Chem. 278*, 50175−50181.
(44) Morrissey, M., and Shakhnovich, E. (1999) Evidence for the role of PrP^{C} helix 1 in the hydrophilic seeding of prion aggregates. *Proc. Natl. Acad. Sci. U.S.A. 96*, 11293−11298.
(45) De Simone, A., Zagari, A., and Derreumaux, P. (2007) Structural and hydration properties of the partially unfolded states of the prion protein. *Biophys. J. 93*, 1284−1292.
(46) Hosszu, L. P., Tattum, M. H., Jones, S., Trevitt, C. R., Wells, M. A., Waltho, J. P., Collinge, J., Jackson, G. S., and Clarke, A. R. (2010) The H187R Mutation of the Human Prion Protein Induces Conversion of Recombinant Prion Protein to the PrP(Sc)-like Form. *Biochemistry 49*, 8729−8738.
(47) Bae, S.-H., Legname, G., Serban, A., Prusiner, S. B., Wright, P. E., and Dyson, H. J. (2009) Prion Proteins with Pathogenic and Protective Mutations Show Similar Structure and Dynamics. *Biochemistry 48*, 8120−8128.
(48) Kuwata, K., Nishida, N., Matsumoto, T., Kamatari, Y. O., Hosokawa-Muto, J., Kodama, K., Nakamura, H. K., Kimura, K., Kawasaki, M., Takakura, Y., Shirabe, S., Takata, J., Kataoka, Y., and Katamine, S. (2007) Hot spots in prion protein for pathogenic conversion. *Proc. Natl. Acad. Sci. U.S.A. 104*, 11921−11926.
(49) Billeter, M., Riek, R., Wider, G., Hornemann, S., Glockshuber, R., and Wuthrich, K. (1997) Prion protein NMR structure and species barrier for prion diseases. *Proc. Natl. Acad. Sci. U.S.A. 94*, 7281−7285.
(50) Hosszu, L. P., Trevitt, C. R., Jones, S., Batchelor, M., Scott, D., Jackson, G. S., Collinge, J., Waltho, J. P., and Clarke, A. R. (2009) Conformational Properties of β-PrP. *J. Biol. Chem. 284*, 21981−21990.
(51) Blinov, N., Berjanskii, M., Wishart, D., and Stepanova, M. (2009) Structural domains and main-chain flexibility in prion proteins. *Biochemistry 48*, 1488−1497.
(52) Santo, K. P., Berjanskii, M., Wishart, D. S., and Stepanova, M. (2011) Comparative analysis of essential collective dynamics and NMR-derived flexibility profiles in evolutionarily diverse prion proteins. *Prion 5*, 188−200.
(53) Hosszu, L., Baxter, N., Jackson, G., Power, A., Clarke, A., Waltho, J., Craven, C., and Collinge, J. (1999) Structural mobility of the human prion protein probed by backbone hydrogen exchange. *Nat. Struct. Biol. 6*, 740−743.
(54) OSullivan, D. B. D., Jones, C. E., Salama, R. A., Brazier, M. A., Toms, H., Brown, D. R., and Viles, J. (2008) Dynamics of a truncated prion protein, PrP(113231), from ^{15}N NMR relaxation: Order parameters calculated and slow conformational fluctuations localized to a distinct region. *Protein Sci. 18*, 410−423.
(55) Biljan, I., Ilc, G., Giachin, G., Raspadori, A., Zhukov, I., Plavec, J., and Legname, G. (2011) Toward the Molecular Basis of Inherited Prion Diseases: NMR Structure of the Human Prion Protein with V210I Mutation. *J. Mol. Biol. 412*, 660−673.
(56) Govaerts, C., Wille, H., Prusiner, S., and Cohen, F. (2004) Evidence for assembly of prions with left-handed β 3-helices into trimers. *Proc. Natl. Acad. Sci. U.S.A. 101*, 8342−8347.
(57) DeMarco, M., and Daggett, V. (2004) From conversion to aggregation: Protofibril formation of the prion protein. *Proc. Natl. Acad. Sci. U.S.A. 101*, 2293−2298.